Article

# Serine versus Threonine Glycosylation: The Methyl Group Causes a Drastic Alteration on the Carbohydrate Orientation and on the Surrounding Water Shell

Francisco Corzana, Jess H. Busto, Gonzalo Jimnez-Oss, Marisa Garca de Luis, Juan L. Asensio, Jess Jimnez-Barbero, Jess M. Peregrina, and Alberto Avenoza

*J. Am. Chem. Soc.*, **2007**, 129 (30), 9458-9467• DOI: 10.1021/ja072181b • Publication Date (Web): 07 July 2007



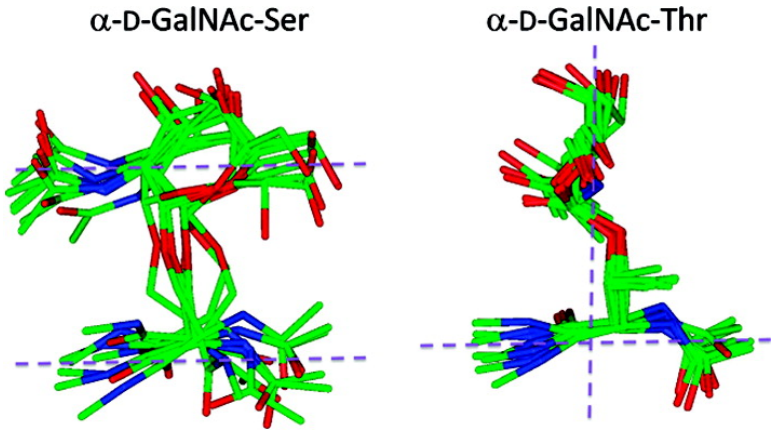


## More About This Article

Additional resources and features associated with this article are available within the HTML version:

- Supporting Information
- Links to the 4 articles that cite this article, as of the time of this article download
- Access to high resolution figures
- Links to articles and content related to this article
- Copyright permission to reproduce figures and/or text from this article

View the Full Text HTML

J|A|C|S
ARTICLES
Published on Web 07/07/2007

# Serine versus Threonine Glycosylation: The Methyl Group Causes a Drastic Alteration on the Carbohydrate Orientation and on the Surrounding Water Shell

Francisco Corzana,*,† Jesús H. Busto,† Gonzalo Jiménez-Osés,† Marisa García de Luis,† Juan L. Asensio,‡ Jesús Jiménez-Barbero,§ Jesús M. Peregrina,† and Alberto Avenoza*,†

*Contribution from Departamento de Química, Universidad de La Rioja, UA-CSIC, Madre de Dios 51, E-26006 Logroño, Spain, Instituto de Química Orgánica (CSIC), Juan de la Cierva 3, E-28006 Madrid, Spain, and Centro de Investigaciones Biológicas (CSIC), Ramiro Maeztu 9, E-28040 Madrid, Spain*

Received March 28, 2007; E-mail: alberto.avenoza@unirioja.es

***Abstract:*** Different behavior has been observed for the $\psi$ torsion angle of the glycosidic linkages of D-GalNAc-Ser and D-GalNAc-Thr motifs, allowing the carbohydrate moiety to adopt a completely different orientation. In addition, the fact that the water pockets found in α-D-GalNAc-Thr differ from those obtained for its serine analogue could be related to the different capability that the two model glycopeptides have to structure the surrounding water. This fact could have important biological inferences (i.e., antifreeze activity).

## Introduction

The most abundant form of *O*-linked glycoproteins in higher eukaryotes, termed "mucin-type", is characterized by α-D-*N*-acetylgalactosamine (α-D-GalNAc) attached to the hydroxyl groups of serine/threonine (Ser/Thr) side chains.[1] These glycoproteins are involved in fundamental biological processes[2] and are attracting a great deal of interest in therapeutic approaches,[3] particularly for the development of vaccines for cancer treatment.[4]

It is well-known that the α-*O*-glycosylation of Ser and Thr has a profound effect on the underlying peptide backbone, forcing it into an extended conformation.[5]

On the other hand, recent studies have indicated that the rotation around the glycosidic linkage in α-D-GalNAc-Thr is restricted, a feature not observed for the Ser-glycosylated analogues,[6] and it has been assumed that this mainly affects the lateral chain of the amino acid residue. However, to the best of our knowledge, the key differences concerning the geometry of the glycosidic linkage and, in particular, the $\Psi_s$ torsion angle have not been reported to date. The way in which these factors could affect the biological behavior of these molecules has also not been studied.

We have observed in the literature[5a,7] that diverse glycopeptides present remarkable differences between the 3D-orientation of the sugar attached to Ser or Thr. Indeed, when Ser is present, the torsion angle $\Psi_s$ of the glycosidic linkage takes a value of around 180°, providing an *anti* arrangement for the bulky GalNAc residue. However, in Thr glycopeptides, $\Psi_s$ frequently adopts a value close to 120°, resulting in the H$\beta$−C$\beta$ and O1s−C1s bonds in an eclipsed conformation (see Figures 1 and 2).

Bearing in mind that this torsional angle ($\Psi_s$) has a primary influence on the orientation of the carbohydrate antenna, a detailed study of the factors that govern the different Ser versus

† Universidad de La Rioja.
‡ Instituto de Química Orgánica (CSIC).
§ Centro de Investigaciones Biológicas (CSIC).

(1) (a) Strous, G. J.; Dekker, J. *Crit. Rev. Biochem. Mol. Biol.* **1992**, *27*, 57−92. (b) Hang, H. C.; Bertozzi, C. R. *Bioorg. Med. Chem.* **2005**, *13*, 5021−5034. (c) Fumoto, M.; Hinou, H.; Ohta, T.; Ito, T.; Yamada, K.; Takimoto, A.; Kondo, H.; Shimizu, H.; Inazu, T.; Nakahara, Y.; Nishimura, S.-I. *J. Am. Chem. Soc.* **2005**, *127*, 11804−11818.

(2) (a) Dwek, R. A. *Chem. Rev.* **1996**, *96*, 683−720. (b) Sears, P.; Wong, C.-H. *Cell Mol. Life Sci.* **1998**, *54*, 223−252. (c) Baldus, S. E.; Engelmann, K.; Hanisch, F.-G. *Crit. Rev. Clin. Lab. Sci.* **2004**, *41*, 189−231. (d) Hanisch, F.-G.; Müller, S. *Glycobiology* **2000**, *10*, 439−449.

(3) (a) Davis, B. G. *Chem. Rev.* **2002**, *102*, 579−601. (b) Watt, G. M.; Lund, J.; Levens, M.; Kolli, V. S. K.; Jefferis, R.; Boons, G.-J. *Chem. Biol.* **2003**, *10*, 807−814. (c) Lui, H.; Wang, L.; Brock, A.; Wong, C.-H.; Schultz, P. G. *J. Am. Chem. Soc.* **2003**, *125*, 1702−1703. (d) Gamblin, D. P.; Garnier, P.; van Kasteren, S.; Oldham, N. J.; Fairbanks, A. J.; Davis, B. G. *Angew. Chem., Int. Ed.* **2004**, *116*, 827−833. (e) Davis, B. G. *Science* **2004**, *303*, 480−482. (f) Dube, D. H.; Bertozzi, C. R. *Nat. Rev. Drug Discovery* **2005**, *4*, 477−488.

(4) (a) Dube, D. H.; Prescher, J. A.; Quang, C. N.; Bertozzi, C. R. *Proc. Natl. Acad. Sci. U.S.A.* **2006**, *103*, 4819−4824. (b) Dziadek, S.; Kunz, H. *The Chem. Rec.* **2004**, *3*, 308−321. (c) Jaracz, S.; Chen, J.; Kuznetsova, L. V.; Ojima, I. *Bioorg. Med. Chem.* **2005**, *13*, 5043−5054. (d) Danishefsky, S. J.; Allen, J. R. *Angew. Chem., Int. Ed.* **2000**, *39*, 836−863. (e) Slovin, S. F.; Ragupathi, G.; Musselli, C.; Olkiewicz, K.; Verbel, D.; Kuduk, S. D.; Schwarz, J. B.; Sames, D.; Danishefsky, S. J.; Livingston, P. O.; Scher, H. I. *J. Clin. Oncol.* **2003**, *21*, 4292−4298. (f) Chen, X.; Lee, G. S.; Zettl, A.; Bertozzi, C. R. *Angew. Chem., Int. Ed.* **2004**, *43*, 6112−6116.

(5) (a) Coltart, D. M.; Royyuru, A. K.; Williams, L. J.; Glunz, P. W.; Sames, D.; Kuduk, S.; Schwarz, J. B.; Chen, X.-T.; Danishefsky, S. J.; Live, D. H. *J. Am. Chem. Soc.* **2002**, *124*, 9833−9844. (b) Pratt, M. R.; Bertozzi, C. R. *Chem. Soc. Rev.* **2005**, *34*, 58−68.

(6) (a) Mimura, Y.; Inoue, Y.; Maeji, N. J.; Chûjô, R. *Int. J. Pept. Protein Res.* **1989**, *34*, 363−368. (b) Naganagowda, G. A.; Gururaja, T. L.; Satyanarayana, J.; Levine, M. J. *J. Pept. Res.* **1999**, *54*, 290−310. (c) Kindahl, L.; Sandström, C.; Norberg, T.; Kenne, L. *Carbohydr. Res.* **2001**, *336*, 319−323. (d) Kogelberg, H.; Solis, D.; Jiménez-Barbero, J. *Curr. Opin. Struct. Biol.* **2003**, *13*, 646−653.

(7) (a) Tachibana, Y.; Fletcher, G. L.; Fujitani, N.; Tsuda, S.; Monde, K.; Nishimura, S.-I. *Angew. Chem., Int. Ed.* **2004**, *43*, 856−862. (b) Yeh, Y.; Feeney, R. E. *Chem. Rev.* **1996**, *96*, 601−617. (c) Ben, R. N. *ChemBioChem* **2001**, *2*, 161−166.


**10.1021/ja072181b CCC: $37.00** 

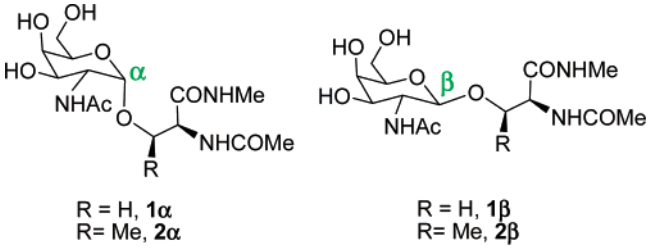


R = H, **1α**
R= Me, **2α**

R = H, **1β**
R= Me, **2β**

***Figure 1.*** Model glycopeptides.

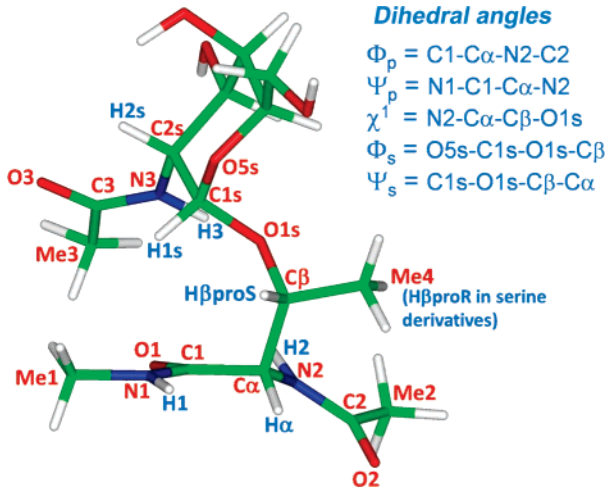


***Figure 2.*** Molecular structure of compound **2α**, showing definitions of the torsional angles and the numbering of the atoms. The same definitions were used for the other model glycopeptides.

Thr conformational behavior of glycopeptides is of paramount importance. Indeed, these differences could play a significant role in their distinct biological functions. For example, it is known that when Ser replaces Thr in a sequence of an antifreeze protein, the resulting structure cannot act as a freezing inhibitor.[7]

We report here the synthesis and the conformational study in aqueous solution of the simplest model glycopeptides derived from Thr and Ser, compounds **1α**, **2α**, **1***β*, and **2***β* (Figure 1). Compound **1α** has recently been reported by our group,[8] while compounds **1***β* and **2***β* were used as models to ascertain whether the eclipsed conformation mentioned above depends on the anomeric center.

## Results

**Synthesis.** The synthesis of the target glycosides **2α**, **1***β*, and **2***β* (Scheme 1) was carried out following the Schmidt procedure[9] that involves a Michael-type addition of the amino acid derivatives **1**, **2**, or **3** (Scheme 1), which were previously prepared by our group,[10] to tri-*O*-benzyl-2-nitro-D-galactal. Therefore, the treatment of protected serine **1** with this nitrogalactal in the presence of $Et_3N$ as a base gave **4***β* as the major product. Then, reduction of the nitro group with Raney nickel T4/$H_2$ and *N*-acetylation gave derivative **5***β*, after column chromatography. Further removal of the benzyl groups afforded glycoside **1***β*.

Compound **2α** was synthesized in a similar way but by using $^t$BuOK as a base in the Michael-type addition. Therefore, compound **2** was transformed into the α-anomer (compound **6α**) with a 58% yield. Transformation of the different groups, using a similar methodology to that described above, led to compound **2α** in a good yield.

Finally, we used the thioglycoside strategy developed by Schmidt and co-workers[11] to obtain **2***β*. In this case, we used compound **3** as the starting material, and the reaction of compound **3** with the thioglycoside shown in Scheme 1 gave compound **6***β* in a moderate yield. Then, the removal of the Boc group with TFA, and further transformation of the nitro group into the corresponding amine, gave, after *N*-acetylation, derivative **8***β*. Finally, this compound was transformed into the desired model glycopeptide **2***β* in a moderate yield.

**NMR Experiments.** The conformational analysis of all the compounds was carried out using NMR spectroscopy. NOE and homonuclear *J* couplings were interpreted with the assistance of molecular dynamics (MD) simulations. The resulting torsional angles and the numbering used in this work for the model compounds are shown in Figure 2.

In a first step, full assignment of the protons in all of the compounds was carried out using COSY and HSQC experiments. Selective 1D-NOESY experiments in $D_2O$ (20 °C, pH = 5.2) and 2D-NOESY experiments in $H_2O/D_2O$ (9/1) (20 °C, pH = 5.2) were then carried out for the model glycopeptides (see Supporting Information and Figure 3). Distances involving NH protons were semiquantitatively determined by integrating the volume of the corresponding cross-peaks. In addition, $^3J$ coupling constants were measured from the splitting of the resonance signals in the 1D spectra and are gathered in Tables 1 and 2. These experimental data were used as restraints in MD simulations.

The thorough study of the 2D NOESY spectra of **2α**, **1***β*, and **2***β* reveals that they present similar NOE patterns. Moreover, this pattern was similar to that previously reported for the model peptides (serine and threonine diamides)[10] and also for the model glycopeptide **1α**.[8] The strong NOE observed between Hα and NH1, along with a medium NOE between NH1 and NH2, suggests the existence of extended conformations in the peptide backbone of all the model glycopeptides (Figure 3).

**MD Simulations**. An experimentally derived ensemble of **2α**, **1***β*, and **2***β* was obtained by carrying out 80-ns MD-tar[12] (MD with time-averaged restraints) simulations including the coupling constants and distances shown in Tables 1 and 2 as time-averaged restraints. The simulations were performed without explicit solvent, but by using a bulk dielectric constant of 80 to reproduce the water environment. In addition, 4 ns MD-tar simulations in explicit water [MD-tar ($H_2O$) in Table 1], as well as 20 ns unrestrained MD simulations in explicit water (see Supporting Information), were also carried out for compound **2α** to compare its hydration shell with that previously reported[10] for the model glycopeptide **1α** (see Supporting Information). As previously observed for **1α**,[8] the unrestrained MD simulations failed to accurately reproduce the conformation of the peptide backbone of **2α**, suggesting a folded conformation (distance NH1−NH2 < distance Hα−NH1). This result is characteristic of the AMBER force field, used in the simulations, which favors helical structures for small peptides as is described in the literature.[13]

(8) Corzana, F.; Busto, J. H.; Jiménez-Osés, G.; Asensio, J. L.; Jiménez-Barbero, J.; Peregrina, J. M.; Avenoza, A. *J. Am. Chem. Soc.* **2006**, *128*, 14640−14648.
(9) Barroca, N.; Schmidt, R. R. *Eur. J. Org. Chem.* **1999**, 1167−1171.
(10) Corzana, F.; Busto, J. H.; Engelsen, S. B.; Jiménez-Barbero, J.; Asensio, J. L.; Peregrina, J. M.; Avenoza, A. *Chem. Eur. J.* **2006**, *12*, 7864−7871.
(11) Barroca, N.; Schmidt, R. R. *Org. Lett.* **2004**, *6*, 1551−1554.
(12) Pearlman, D. A. *J. Biomol. NMR* **1994**, *4*, 1−16.
(13) Gnanakaran, S.; Garcia, A. E. *J. Phys. Chem. B* **2003**, *107*, 12555−12557.

***Scheme 1.*** Synthetic Routes to **1**$\beta$, **2**$\alpha$, and **2**$\beta$.

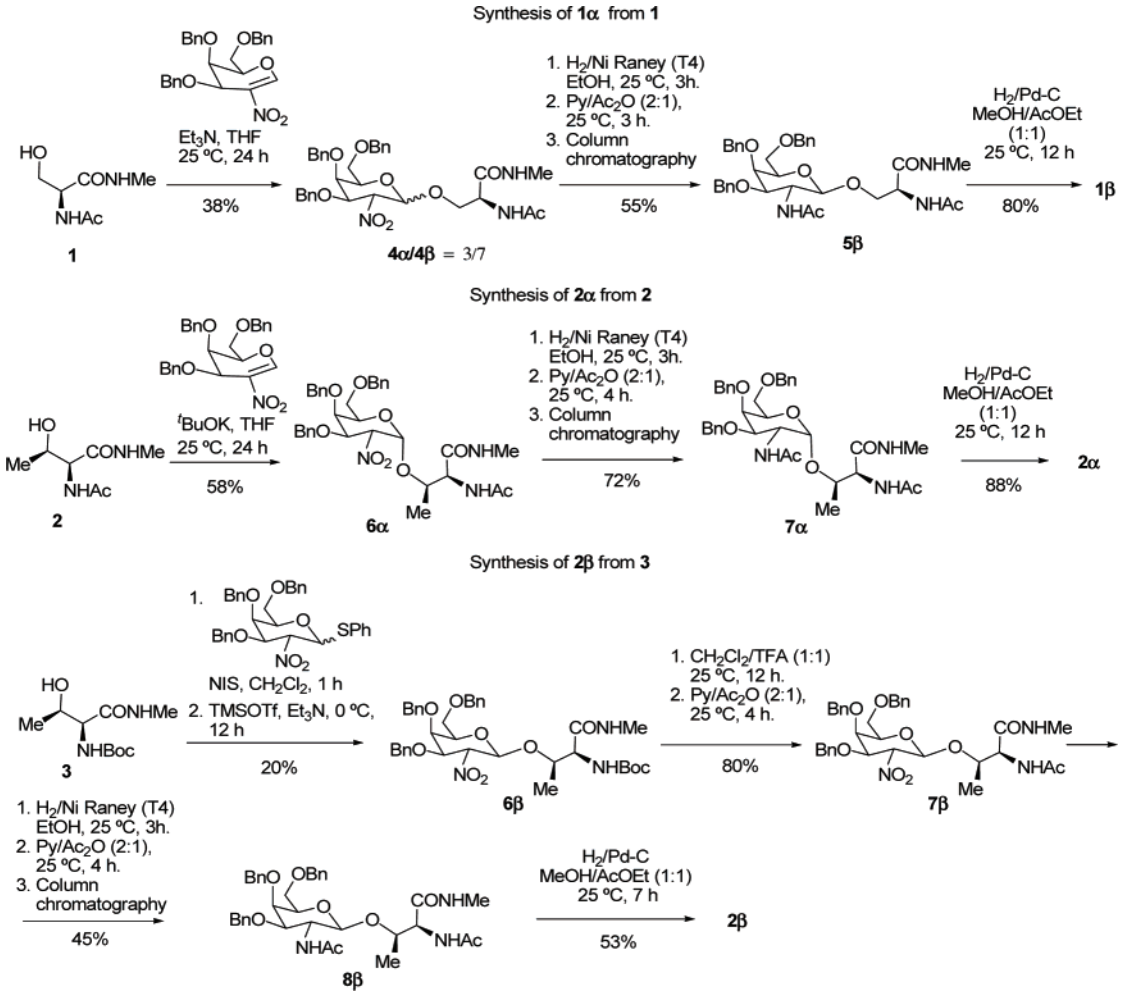


The calculated $^3J$ coupling constant values were obtained from the simulations by applying the appropriate Karplus equation[14] to the corresponding torsion angles. As can be seen in Tables 1 and 2, both the distances and calculated $^3J_{H,H}$ values from the simulations are in very good agreement with the experimental ones.

The distribution for the peptide backbone ($\Phi_p/\Psi_p$) of the model glycopeptides, obtained from the MD-tar simulations, is shown in Figure 4. It can be seen that, according to the NOE experiments mentioned above, the $\Phi_p/\Psi_p$ dihedral values (backbone) of these models are similar to typical values for extended conformations, such as PPII and $\beta$-sheet, and only a small number of conformers showed $\Phi_p/\Psi_p$ dihedral values corresponding to an $\alpha$-helical conformation. These results suggest that the *O*-glycosylation with GalNAc (via $\alpha$- or $\beta$-) of Ser and Thr diamides does not significantly affect the conformation of the peptide backbone of the *underlying amino acid*.

As far as the lateral chain ($\chi^1$ torsional angle) is concerned, the model glycopeptides derived from Thr, **2**$\alpha$ and **2**$\beta$, show $^3J_{H\alpha,H\beta}$ values that are smaller than those observed for the Ser analogues; such values have previously been observed for larger glycopeptides.[6]

This fact suggests that rotation around $\chi^1$ in the Thr derivatives is to some extent restricted. On this basis, the distribution of the lateral chain ($\chi^1$ torsional angle) obtained for the $\alpha$ and $\beta$ anomers from the MD-tar simulations is shown in Figure 5. Interestingly, the most stable rotamer presents a value for $\chi^1$ close to 60° in all of the compounds. This result is consistent with the medium observed NOE between the acetamide methyl (Me3) of the carbohydrate residue and the methyl amide (Me1) of the peptide moiety in compounds **1**$\alpha$[8] and **2**$\alpha$ (see Supporting Information). As shown in Figure 5, the extra rigidity of the lateral chain is especially remarkable in compound **2**$\alpha$, in which only the gauche(+) conformer was observed.

The distribution of the glycosidic linkages ($\Phi_s/\Psi_s$) obtained for all the model glycopeptides from the MD-tar simulations is shown in Figure 6. In this case, both torsional angles are, in some way, restricted. With regard to $\Phi_s$, this angle has a value of around 60° for the $\alpha$ anomers and close to −60° for the $\beta$ derivatives, which is in good agreement with the exo-anomeric effect. However, Ser and Thr derivatives showed markedly different behavior in terms of the $\Psi_s$ dihedral angle. Remarkably, in Thr-compounds **2**$\alpha$ and **2**$\beta$, $\Psi_s$ was rather rigid with values mainly close to 120°, resulting in the H$\beta$−C$\beta$ and O1s−C1s bonds in an eclipsed conformation. In contrast, in Ser-glycopeptides, $\Psi_s$ was more flexible, providing in most of the cases an *anti* arrangement for the GalNAc residue regarding the peptide moiety. This result was independent of the configuration at the anomeric center. Moreover, this result appears to

(14) (a) Marco, A.; Llinas, M.; Wuthrich, K. *Biopolymers* **1978**, *17*, 617−636. (b) Vuister, G. W.; Bax, A. *J. Am. Chem. Soc.* **1993**, *115*, 7772−7777.

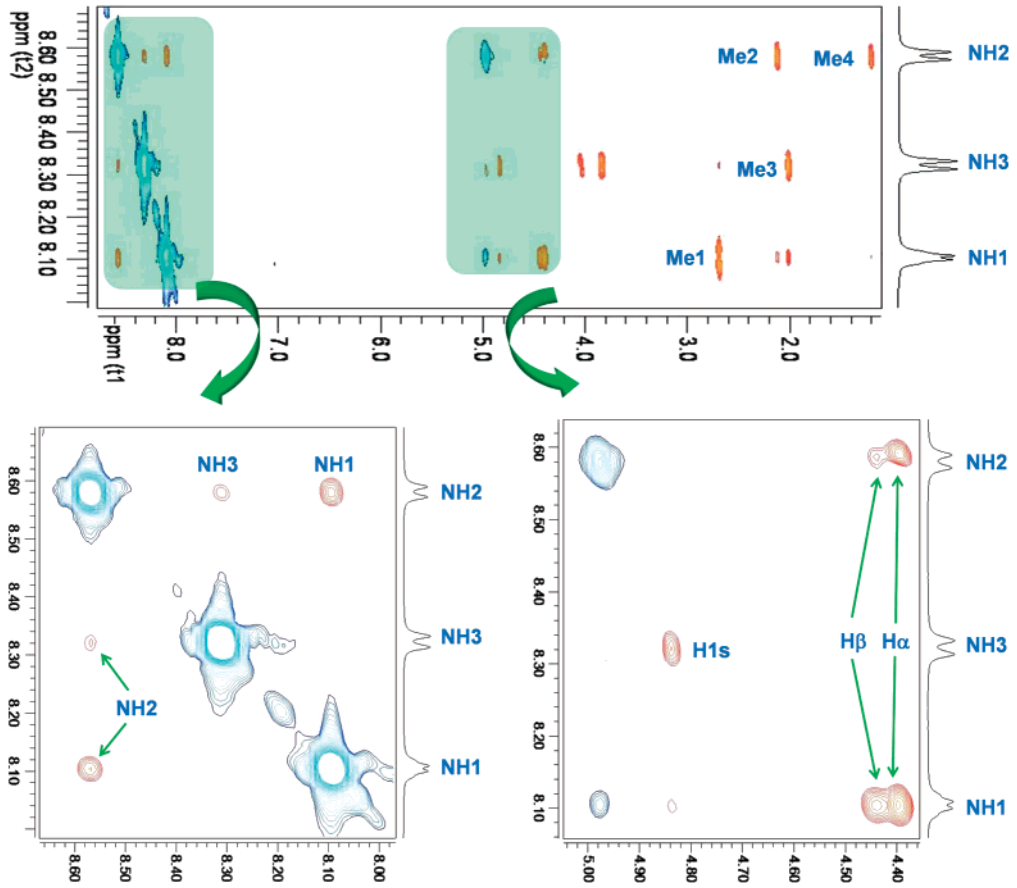


***Figure 3.*** Section of the 800 ms 2D NOESY spectrum (500 MHz) in $H_2O/D_2O$ (9:1) at 25 °C of model glycopeptide **2**α, showing the amide cross-peaks NH1, NH2, and NH3. Diagonal peaks and exchange cross-peaks connecting NH protons and water are negative (blue color). The NOE contacts are represented as positive cross-peaks (red color).

***Table 1.*** Comparison of the Experimental and MD Simulation Derived Distances and $^3J$ Coupling Constants for **2**α

| | exptl[a] | MD-tar ($\epsilon = 80$) | MD-tar ($H_2O$) |
|---|---|---|---|
| $d_{NH1,NH2}$ | 2.8[b] | 2.8 | 2.8 |
| $d_{NH2,NH3}$ | 3.3[b] | 3.1 | 3.2 |
| $d_{H\alpha,NH1}$ | 2.4[b] | 2.5 | 2.5 |
| $d_{H\alpha,NH2}$ | 2.9[b] | 2.8 | 2.9 |
| $d_{H\beta,NH1}$ | 2.8[b] | 2.6 | 2.6 |
| $d_{H\beta,NH2}$ | 3.5[b] | 3.5 | 3.7 |
| $^3J_{H\alpha,H\beta}$ | 2.5 | 2.8[c] | 3.2[c] |
| $^3J_{H\alpha,NH2}$ | 8.8 | 8.1[d] | 7.9[d] |
| $^3J_{H2s,NH3}$ | 9.5 | 9.2[d] | 9.4[d] |

[a] Distances are given in Å and $^3J$ coupling constants in Hz. [b] Distances involving NH protons were semiquantitatively determined by integrating the volume of the corresponding cross-peaks. [c] Estimated using the Karplus equation given in ref 14a. [d] Estimated using the Karplus equation given in ref 14b.

***Table 2.*** Comparison of the Experimental and MD Simulation Derived Distances and $^3J$ Coupling Constants for **1**$\beta$ and **2**$\beta$

| | compound **1**$\beta$ | | compound **2**$\beta$ | |
|---|---|---|---|---|
| | exptl[a] | MD-tar ($\epsilon = 80$) | exptl[a] | MD-tar ($\epsilon = 80$) |
| $d_{NH1,NH2}$ | 2.9[b] | 2.9 | 3.0[b] | 2.9 |
| $d_{H\alpha,NH1}$ | 2.2[b] | 2.3 | 2.3[b] | 2.5 |
| $d_{H\alpha,NH2}$ | 2.6[b] | 2.8 | 2.8[b] | 2.9 |
| $d_{H\beta proR,NH2}$ | 2.6[b] | 2.7 | | |
| $d_{H\beta proS,NH2}$ | 2.8[b] | 2.7 | [e] | 2.5 |
| $^3J_{H\alpha,H\beta proR}$ | 6.8 | 6.4[c] | | |
| $^3J_{H\alpha,H\beta proS}$ | [e] | 5.6[c] | 3.5 | 3.6[c] |
| $^3J_{H\alpha,NH2}$ | 6.6 | 6.5[d] | 7.4 | 7.1[d] |
| $^3J_{H2s,NH3}$ | 9.6 | 9.3[d] | 9.9 | 9.3[d] |

[a] Distances are given in Å and $^3J$ values in Hz. [b] Distances involving NH protons were semiquantitatively determined by integrating the volume of the corresponding cross-peaks. [c] Estimated by using the Karplus equation given in ref 14a. [d] Estimated by using the Karplus equation given in ref 14b. [e] Not determined due to overcrowded NMR spectrum.

be independent of the carbohydrate moiety. A similar result was obtained for model $\beta$-*O*-glucopeptides previously reported by our group.[10]

As a consequence of the different $\Psi_s$ values in Thr and Ser derivatives, the carbohydrate moiety adopts a completely different orientation. Thus, while in compound **2**α, the carbohydrate moiety is almost perpendicular to the peptide backbone; in **1**α the GalNAc adopts a parallel disposition (Figure 7). As a consequence, the *N*-acetyl group of the carbohydrate in **2**α is in close proximity to the peptide backbone (see structure of **2**α in Figure 6).

**Solvent Influence on the Conformational Behavior of Compound 2α and DFT Calculations.** Interestingly, the orientation of the carbohydrate in **2**α allows weak hydrogen bonding between the amide proton of the GalNAc (dubbed NH3) and the carbonyl oxygen of the *O*-linked Thr residue (O1). Thus, while this hydrogen bonding was present for about 8% of the total trajectory time in **2**α, it was never detected for **1**α during the course of the MD simulations.[8] This finding was also reported by Gururaja and co-workers,[6b] who stated that the intramolecular hydrogen bonding in Thr-glycopeptides is the key structure stabilizing element. However, we think that the

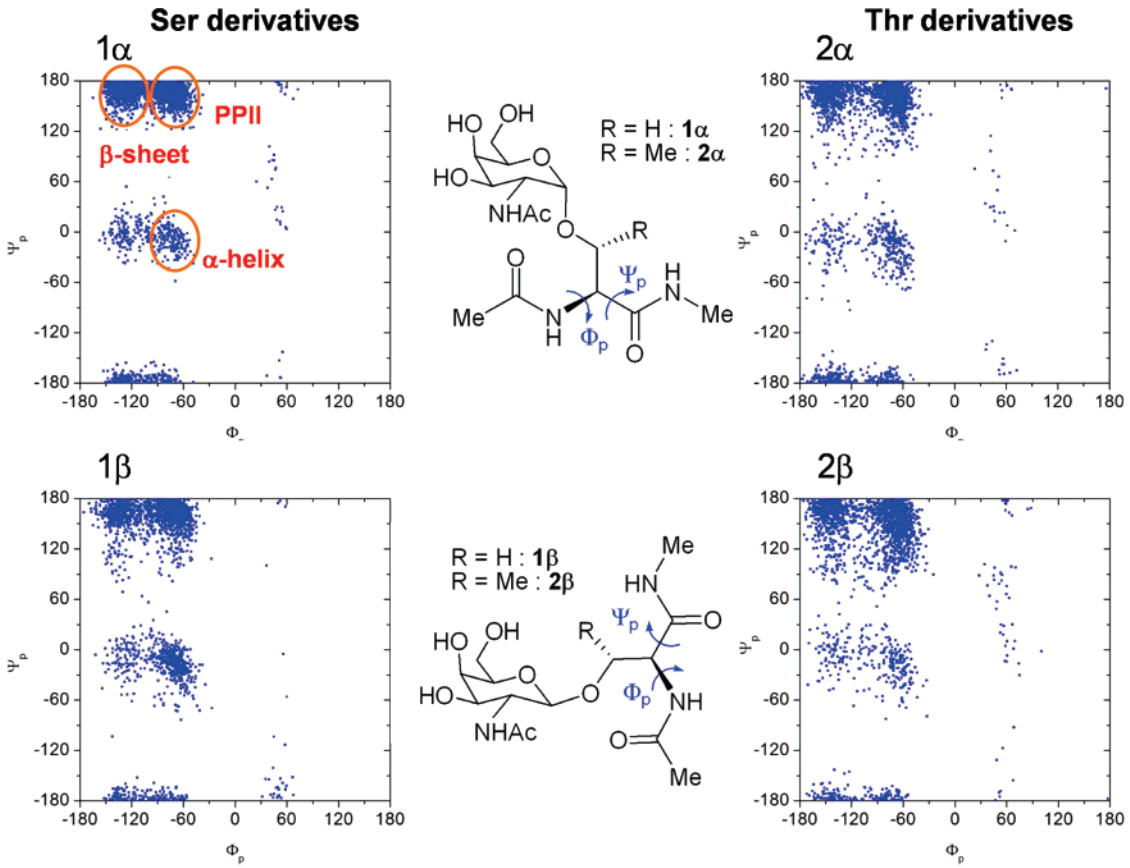


***Figure 4.*** Distributions for the simulated peptide backbone ($\Phi_p/\Psi_p$) of the model glycopeptides obtained from the MD-tar simulations.

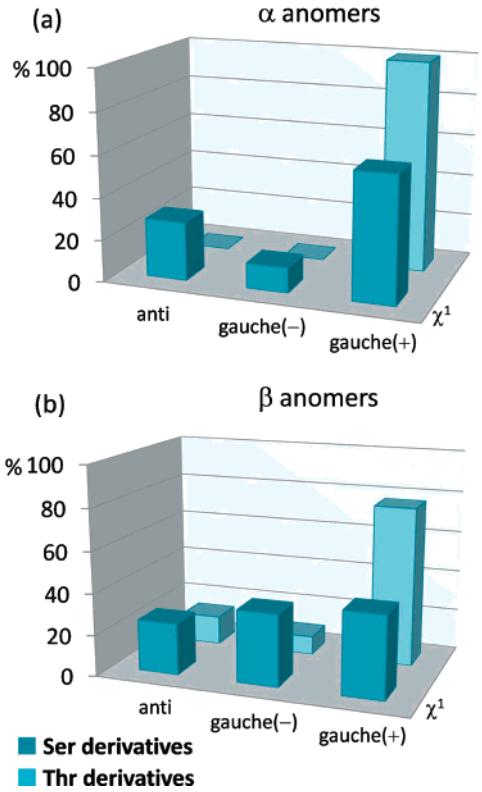


***Figure 5.*** Distributions for the lateral chain ($\chi^1$) of the model glycopeptides **1**α and **2**α (a) and **1**$\beta$ and **2**$\beta$ (b) obtained from the MD-tar simulations.

absence of NOEs between the *N*-acetyl group of the GalNAc and NH1 and/or Me1 indicates that the hydrogen bond must be very weak and, as a consequence, it should not be responsible for the defined conformation of the model glycopeptide. On the other hand, and due to the proximity of the carbohydrate and the peptide moieties, it is not possible to accommodate any water pockets/bridges in the neighborhood of NH3 and O1, unlike the situation reported for **1**α.[8] In contrast, an interesting water pocket was found between NH3 and NH2 (Figure 8a), which was in good agreement with the NOE observed between these two protons (Figure 3). A strikingly similar NOE has been observed in MUC1 derivatives recently synthesized by Kunz and co-workers.[15] The density of this shared water site was 6.2 times the bulk density, having maximum and average residence times of 9.5 and 1.0 ps. Interestingly, the fact that the water pockets found in Thr derivative **2**α differ from those previously obtained for its Ser analogue **1**α could be related to the different capabilities that α-D-GalNAc-Ser and α-D-GalNAc-Thr motifs have to structure the surrounding water. Therefore, this finding could have important biological implications (i.e., antifreeze activity).[7a] In this sense, although the mechanism of action of the antifreeze proteins at molecular level still remains to be elucidated, the current hypothesis indicates that the antifreeze activity could be related with the irreversible binding of the antifreeze molecules to the ice surface through a hydrogen-bonding network.[7b] Presumably, and attending to the fact that the water pockets found in **2**α are more persistent than those observed in **1**α, this hydrogen-bonding network should be more efficient in **2**α, which could explain to some extent why the Thr residues are necessary to maintain the antifreeze activity.

(15) Dziadek, S.; Griesinger, C.; Kunz, H.; Reinscheid, U. M. *Chem. Eur. J.* **2006**, *12*, 4981−4993.

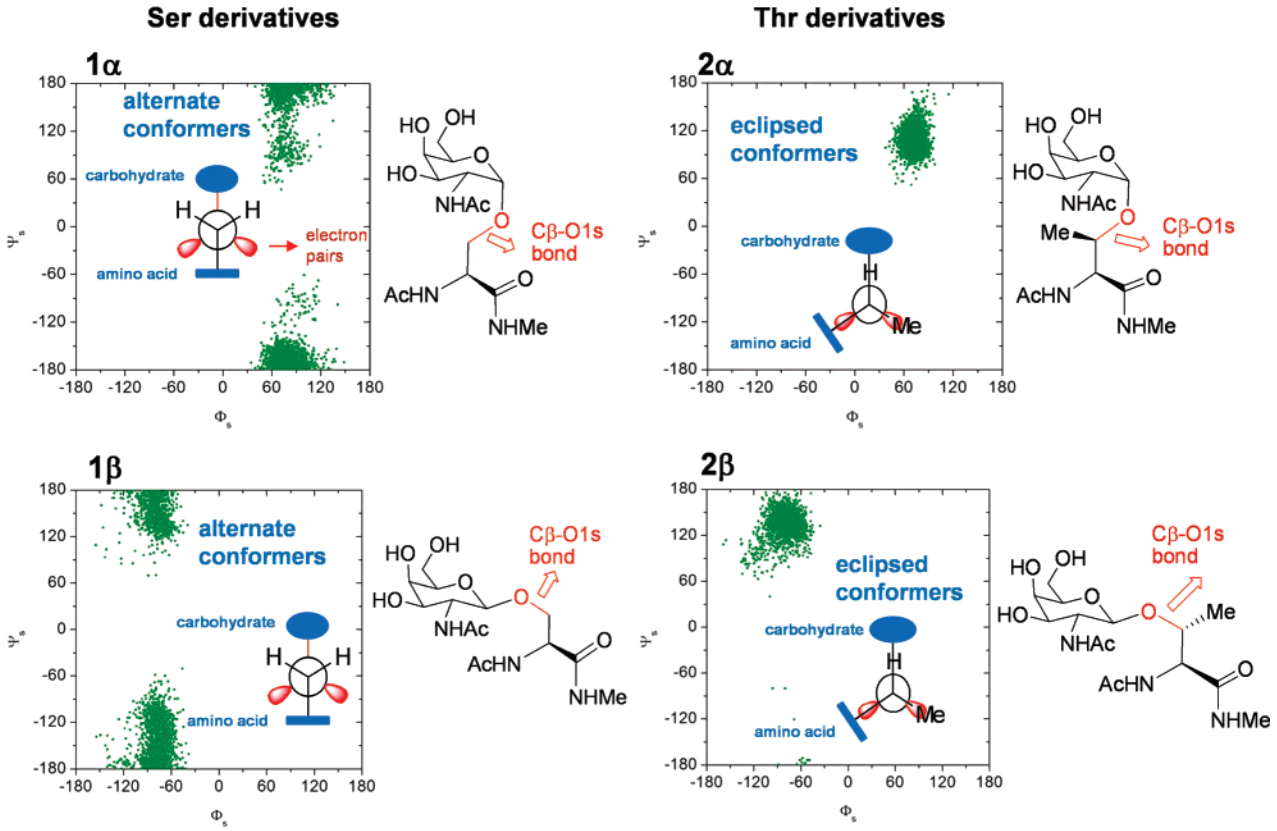


***Figure 6.*** Distributions of the glycosidic linkage ($\Phi_s/\Psi_s$) of the model glycopeptides obtained from the MD-tar simulations. Newman projections of the C$\beta$−O1s bond are included into the diagrams.

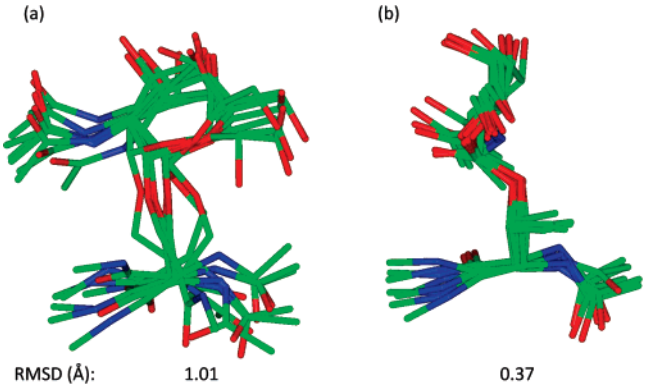


***Figure 7.*** Calculated ensembles for compounds **1**α (a) and **2**α (b) obtained from the MD-tar simulations, showing the RMSDs for heavy atom superimposition.

On the other hand, our experience[8] has demonstrated that the combination of several methodologies is required to reach reasonable conclusions consistent with the experimental data. The combination of MD-tar simulations in explicit water followed by DFT optimization of frames of the MD trajectory has shown to be the most expedient and practical procedure to obtain accurate geometries of the model glycopeptides together with the first solvation shell. This protocol allows us to evaluate both the influence of the surrounding water in the solute geometry, and also the influence of the solute on the organization of the surrounding water. Therefore, a reliable structure for compound **2**α was obtained, according to our previously established protocol,[8] by optimizing, through DFT methods, a frame of the MD simulations in explicit water, in which the model glycopeptide shows an extended conformation. As mentioned above, the inclusion of water molecules from the first solvation shell was required to obtain a structure compatible with the experimental data. As can be seen in Figure 8b, the DFT optimized structure of model glycopeptide **2**α shows an extended conformation for the backbone and an eclipsed conformation around $\psi_s$ (the alternate one could not be located through this methodology). Notably, this result corroborates the conformational preferences obtained from the MD simulations. Furthermore, DFT calculations demonstrated that the existence of bridging water molecules is not only possible but necessary to stabilize the experimentally observed geometries.

Although it seems rather unusual that a rotamer containing eclipsed atoms is found to be the most stable one, a survey of the Cambridge Structural Data Base revealed several structures (CSD refcodes: DMGALP, RONHEH, and ZOSSEF) that contain eclipsed H−C−O−C torsional angles.[16] Moreover, some carbohydrates containing eclipsed structures have been recently reported, from a theoretical point of view.[17] To gain some insights into the behavior of the glycosidic linkage in Ser/Thr model glycopeptides, we carried out a thorough theoretical study of their intrinsic conformational preferences using the reduced models shown in Figure 9.

Relaxed PES scans at the B3LYP/6-31G(d,p) level along the $\Psi_s$ dihedral angle were performed for these models of **1**α and **2**α. As can be seen in Figure 9b, the double-minimum potential calculated for the α-Glyco-Ser model agrees quite well with the experimental data previously reported for α-D-GalNAc-Ser,

(16) Allen, F. H.; Davis, J. E.; Galloy, J. J.; Johnson, O.; Kennard, O.; Macrae, C. F.; Mitchell, E. M.; Mitchell, G. F.; Smith, J. M.; Watson, D. G. *J. Chem. Inf. Comput. Sci.* **1991**, *31*, 187−204.
(17) Csonka, G. I.; Schubert, G. A.; Perczel, A.; Sosa, C. P.; Csizmadia, I. G. *Chem. Eur. J.* **2002**, *8*, 4718−4733.

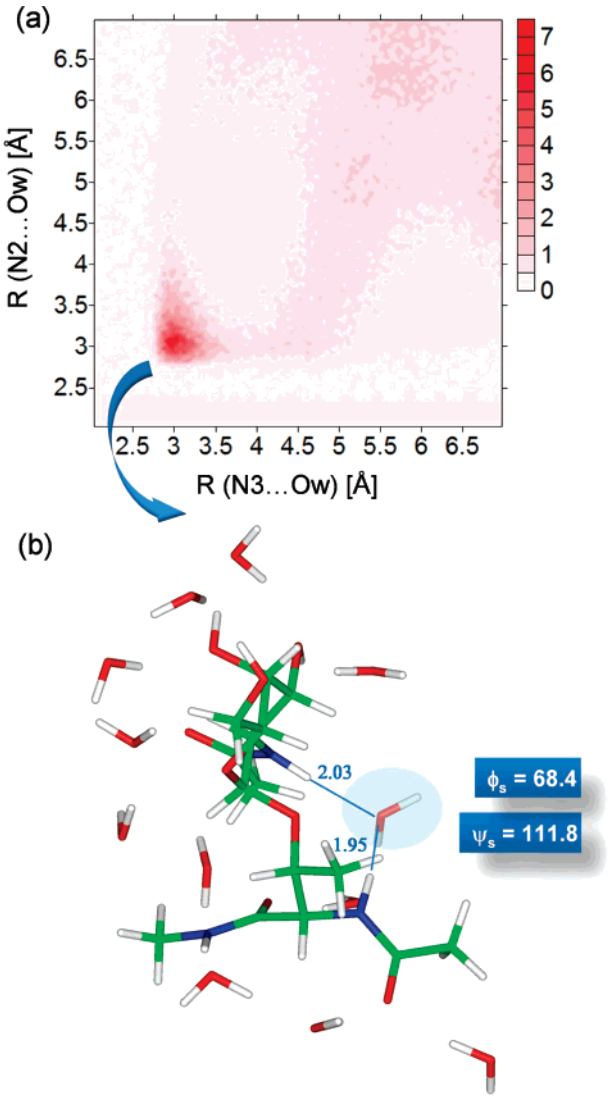


***Figure 8.*** (a) Two-dimensional radial pair distribution function for N2 and N3 found in the 4 ns $MD_{H2O}$-tar simulation of **2**α. (b) Calculated B3LYP/6-31G(d) geometry of compound **2**α, including the surrounding water molecules. Distances are given in ångstroms and torsion angles in degrees.

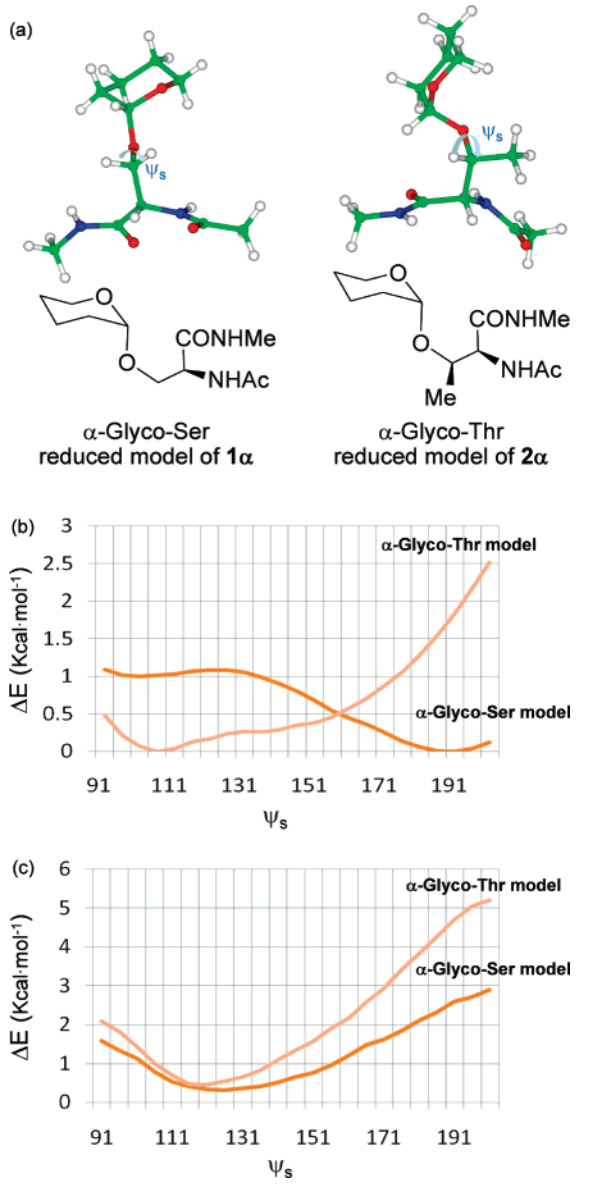


***Figure 9.*** (a) Three-dimensional structure of the reduced model for **1**α and **2**α. (b) PES of α-Glyco-Ser and α-Glyco-Thr reduced models. (c) Long-range effects in α-Glyco-Ser and α-Glyco-Thr reduced models. All quantities were calculated at the B3LYP/6-31G(d,p) level.

with the alternate conformation ($\psi_s$ = 190°) being the most stable one. In the case of the α-Glyco-Thr model, only one minimum with an eclipsed conformation ($\psi_s$ = 105°) was found. In this case, the alternate conformations were clearly inaccessible.

**Origin of the Conformational Preferences.** We would like to point out that the influence of the methyl group on the torsional energy profiles around the Ψ angles is not at the origin of the different orientation detected for the carbohydrate moiety in compounds **1**α and **2**α. Thus, the minima of the torsional energy of $\Psi_s$, according to AMBER/GLYCAM force field, lay on alternate conformations in both derivatives (see Supporting Information). Therefore, the conformational preferences must be related to other additional stereoelectronic factors other than the simple torsional energy. Since these effects are not easy to evaluate from the MD simulations, the DFT study was carried out. An effort to locate the source of these subtle conformational differences was made by evaluating the steric and delocalizing (hyperconjugative) interactions in both substrates, by means of the NBO partition scheme.[18] These interactions were calculated for both the rotation along $\Psi_s$ (torsional effects) and selected areas of the ring and amino acid moieties (long-range effects), as depicted in the Supporting Information. Hence, whereas the smallest torsional effects were located at alternate conformations around $\Psi_s$, long-range interactions were minima at the eclipsed ones in both structures. The driving force for the extra stabilization of the α-Glyco-Thr model at the eclipsed conformations is, therefore, the greater long-range effects arising at values of $\Psi_s$ close to 180°, which arise due to the growing steric repulsions between the ring moiety (principally the lone pairs of the endocyclic oxygen O5s) and the $\beta$-methyl group (Figures 9c and 10). In contrast to the α-Glyco-Ser model, these long-range interactions clearly overcome the torsional preferences

(18) Glendening, E. D.; Badenhoop, J. K.; Reed, A. E.; Carpenter, J. E.; Bohmann, J. A.; Morales, C. M.; Weinhold, F. *NBO 5.0*; Theoretical Chemistry Institute, University of Wisconsin: Madison, WI, 2001.

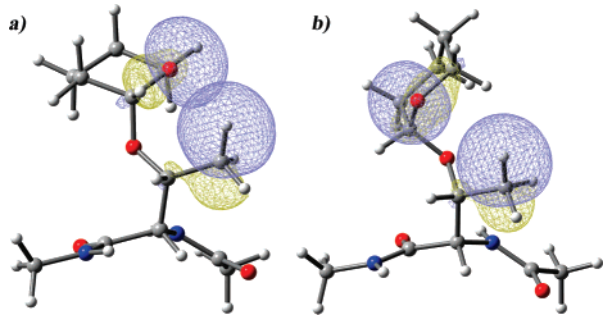


***Figure 10.*** Three-dimensional plots of the $\sigma_{C-H}$ ($\beta$-methyl group) and $n^1_O$ (endocyclic oxygen) NBOs of the α-Glyco-Thr reduced model, calculated at the B3LYP/6-31G(d,p) level, corresponding to representative (a) alternate ($\Psi_s = 180°$) and (b) eclipsed ($\Psi_s = 120°$) conformations.

in the α-Glyco-Thr one and consequently force it to adopt an eclipsed conformation close to 120°.

**Conclusions.** We have synthesized and carried out a thorough conformational analysis of the simplest model glycopeptides. Strikingly different behavior was observed for the $\psi$ torsion angle of the glycosidic linkages of D-GalNAc-Ser (alternate conformations) or D-GalNAc-Thr (eclipsed conformations) motifs present in natural glycopeptides. Moreover, we have demonstrated that this exceptional behavior of the glycosidic linkage is independent of the anomeric center (α or $\beta$). On the other hand, although in the Thr derivative **2**α the carbohydrate and backbone moieties are closer than in the Ser derivative **1**α, the hydrogen bond between these moieties is very weak, as inferred from NMR data and MD simulations. Consequently, hydrogen bonding cannot be responsible for the extended conformation of the backbone. In addition, the rigidity of **2**α is, as for **1**α, well explained by the presence of water pockets/bridges between the carbohydrate and the peptide moieties. Interestingly, the water pockets found in **2**α differ from those previously deduced for its Ser analogue. This finding suggests that the α-D-GalNAc-Ser and α-D-GalNAc-Thr motifs structure the surrounding water in rather different ways, which could explain the loss of activity of an antifreeze protein (α-D-GalNAc-Ser/Thr-Ala-Ala) when the Thr is replaced by the Ser.[7] Finally, a DFT study allowed us to identify the stereoelectronic origin of the conformational preferences for **2**α by evaluating both the torsional and the long-range effects on the $\Psi_s$ values. The obtained results indicate that the different behavior observed for the glycosidic linkage in the Thr versus Ser derivatives can be explained in terms of steric repulsions between the carbohydrate moiety (endocyclic oxygen) and the $\beta$-methyl group in the former, forcing them to be located far away from each other in the molecule, which causes an eclipsed conformation of the $\Psi_s$ torsion angle.

## Experimental Section

**General Procedures.** Solvents were purified according to standard procedures. Analytical TLC was performed using Polychrom SI F254 plates. Column chromatography was performed using silica gel 60 (230−400 mesh). Melting points were determined on a Büchi B-545 melting point apparatus and are uncorrected. Optical rotations were measured on a Perkin-Elmer 341 polarimeter. Microanalyses were carried out on a CE Instruments EA-1110 analyzer and are in good agreement with the calculated values. $^1$H and $^{13}$C NMR data were obtained on a Bruker Avance 400 MHz spectrometer.

**Synthesis of Compounds 4α and 4$\beta$.** Compound **1** (100 mg, 0.62 mmol) and tri-*O*-benzyl-2-nitrogalactal (214 mg, 0.46 mmol) were dissolved in THF (5 mL) under argon, and freshly activated molecular sieve (3 Å, 0.6 g) was then added. After the reaction mixture stirred at 25 °C for 30 min, $Et_3N$ (1 mL, 6.9 mmol) was added, and stirring was continued for 24 h. Acetic acid (0.5 mL) was used to acidify the reaction mixture, the molecular sieve was filtered off, and all solvents were removed by evaporation. The residue was purified by silica gel column chromatography (ethyl acetate/methanol, 98:2) to give a mixture of **4**α and **4**$\beta$ in a 3:7 ratio (110 mg), as an oil, in 38% yield. $^1$H NMR (400 MHz, $CDCl_3$) data for this mixture follow: $\delta$ 1.99, 1.98 (s, 3H), 2.76, 2.73 (d, $J$ = 4.8 Hz, 3H), 3.48−3.61 (m, 1H), 3.63−3.71 (m, 1H), 3.89−3.95 (m, 1H), 3.99−4.00 (m, 1H), 4.32−4.62 (m, 6H), 4.66−4.74 (m, 2H), 4.79−4.87 (m, 2H), 5.02 (dd, $J$ = 12.0 Hz, $J$ = 4.0 Hz, 1H), 5.38 (d, $J$ = 4.0 Hz, 1H), 6.17−6.31 (m, 1H), 6.38−6.51 (m, 1H), 7.20−7.38 (m, 15H). Anal. Calcd for $C_{33}H_{39}N_3O_9$: C, 63.76; H, 6.32; N, 6.76. Found: C, 63.85; H, 6.30; N, 6.81.

**Synthesis of Compound 5$\beta$.** Platinized Raney-nickel (T4) catalyst was freshly prepared as described in the literature.[19] The catalyst obtained by using 2 g of Raney nickel/aluminum alloy was suspended in ethanol (10 mL) and pre-hydrogenated for 10 min before the addition of the mixture of glycosides **4**α and **4**$\beta$ (110 mg, 0.18 mmol) in ethanol (7 mL). The reaction mixture was shaken under $H_2$ (1 atm) for 3 h at 25 °C. The catalyst was filtered off and the solvent evaporated. The residue was dissolved in pyridine/acetic anhydride (2:1, 6 mL) and stirred at 25 °C for 3 h. Removal of the volatiles followed by a silica gel column chromatographic purification (ethyl acetate/methanol, 95:5) gave an oily residue corresponding to $\beta$-glycoside **5**$\beta$ (63 mg) in 55% yield. $^1$H NMR (400 MHz, $CDCl_3$): $\delta$ 1.91 (s, 3H), 1.98 (s, 3H), 2.69 (d, $J$ = 4.8 Hz, 3H), 3.59−3.67 (m, 4H), 3.80−3.87 (m, 2H), 3.95 (s, 1H), 4.04 (dd, $J$ = 10.5 Hz, $J$ = 5.2 Hz, 1H), 4.41−4.54 (m, 4 H), 4.57 (d, $J$ = 11.4 Hz, 1H), 4.67 (d, $J$ = 11.9 Hz, 1H), 4.73 (d, $J$ = 7.7 Hz, 1H), 4.88 (d, $J$ = 11.4 Hz, 1H), 5.54 (d, $J$ = 7.1 Hz, 1H), 6.64 (d, $J$ = 3.5 Hz, 1H), 6.72 (d, $J$ = 6.4 Hz, 1H), 7.27−7.39 (m, 15H). $^{13}$C NMR (100 MHz, $CD_3OD$): $\delta$ 23.1, 23.7, 26.3, 52.6, 53.4, 68.4, 68.5, 71.8, 71.9, 73.3, 73.5, 74.5, 78.0, 101.2, 127.9, 128.1, 128.1, 128.3, 128.5, 128.6, 137.6, 137.8, 138.3, 170.2, 170.4, 171.0. Anal. Calcd for $C_{35}H_{43}N_3O_8$: C, 66.33; H, 6.84; N, 6.63. Found: C, 66.41; H, 6.91; N, 6.58.

**Synthesis of Compound 1$\beta$.** To a solution of glycoside **5**$\beta$ (25 mg, 0.04 mmol) in ethyl acetate/methanol (1:1) (3 mL) was added 10% palladium−carbon (12 mg) as a catalyst. The reaction mixture was shaken under $H_2$ (1 atm) for 12 h at 25 °C. Removal of the catalyst and a further purification of the residue with C18 reverse-phase sep-pak cartridge gave **1**$\beta$ (12 mg), as a colorless oil, in 80% yield. $[\alpha]^{25}_D$ = −0.5 ($c$ = 1.29, MeOH). $^1$H NMR (400 MHz, $D_2O$): $\delta$ 1.99 (s, 3H), 2.02 (s, 3H), 2.70 (s, 3H), 3.61−3.70 (m, 2H), 3.71−3.79 (m, 2H), 3.80−3.93 (m, 3H), 3.96−4.04 (m, 1H), 4.36−4.46 (m, 2H). $^1$H NMR (400 MHz, $H_2O/D_2O$, 9:1) for the region of amides: $\delta$ 7.96−8.02 (m, 1H), 8.12 (d, $J$ = 9.6 Hz, 1H), 8.24 (d, $J$ = 6.6 Hz, 1H). $^{13}$C NMR (100 MHz, $D_2O$): $\delta$ 24.1, 24.6, 28.3, 54.6, 56.3, 63.4, 70.1, 70.4, 73.2, 77.5, 103.7, 174.1, 176.8, 177.1. Anal. Calcd for $C_{14}H_{25}N_3O_8$: C, 46.28; H, 6.93; N, 11.56. Found: C, 46.30; H, 6.99; N, 11.52.

**Synthesis of Compound 6α.** Compound **2** (212 mg, 1.22 mmol) and tri-*O*-benzyl-2-nitrogalactal (468 mg, 1.01 mmol) were dissolved in THF (15 mL) under argon, and freshly activated molecular sieve (3 Å, 0.3 g) was then added. After the reaction mixture was stirred at 25 °C for 30 min, 1 M $^t$BuOK solution in THF (102 $\mu$L, 0.1 mmol) was added, and stirring was continued for 24 h. Acetic acid (0.5 mL) was used to acidify the reaction mixture, the molecular sieve was filtered off, and all solvents were removed by evaporation. The residue was purified by silica gel column chromatography (ethyl acetate/methanol, 98:2) to give only the α-anomer **6**α (370 mg), as an oil, in 58% yield. $[\alpha]^{25}_D$ = +112.9 ($c$ = 1.45, $CHCl_3$). $^1$H NMR (400 MHz, $CDCl_3$): $\delta$ 1.16 (d, $J$ = 8.0 Hz, 3H), 2.05 (s, 3H), 2.80 (d, $J$ = 4.0 Hz, 3H), 3.48−3.62 (m, 2H), 3.98−4.07 (m, 2H), 4.30 (dd, $J$ = 8.0 Hz, $J$ = 4.0

(19) Nishimura, S. *Bull. Chem. Soc. Jpn.* **1959**, *32*, 61−64.

Hz, 1H), 4.32−4.51 (m, 5H), 4.68 (dd, $J$ = 20.0 Hz, $J$ = 12.0 Hz, 2H), 4.82 (d, $J$ = 12.0 Hz, 1H), 5.03 (dd, $J$ = 8.0 Hz, $J$ = 4.0 Hz, 1H), 5.56 (d, $J$ = 4.0 Hz, 1H), 6.21−6.26 (m, 1H), 6.38 (d, $J$ = 8.0 Hz, 1H), 7.19−7.37 (m, 15H). $^{13}$C NMR (100 MHz, $CDCl_3$): $\delta$ 17.5, 23.3, 26.4, 56.6, 68.3, 70.2, 72.8, 72.8, 73.7, 74.1, 75.1, 84.9, 96.6, 127.8, 128.0, 128.1, 128.2, 128.4, 128.5, 128.6, 137.1, 137.7, 137.9, 169.2, 170.5. Anal. Calcd for $C_{34}H_{41}N_3O_9$: C, 64.24; H, 6.50; N, 6.61. Found: C, 64.30; H, 6.47; N, 6.58.

**Synthesis of Compound 7α.** Platinized Raney-nickel (T4) catalyst was freshly prepared as described in the literature.[19] The catalyst obtained using 2 g of Raney nickel/aluminum alloy was suspended in ethanol (10 mL) and pre-hydrogenated for 10 min before the addition of **6**α (190 mg, 0.30 mmol) in ethanol (8 mL). The reaction mixture was shaken under $H_2$ (1 atm) for 3 h at 25 °C. The catalyst was filtered off and the solvent evaporated. The residue was dissolved in pyridine/acetic anhydride (2:1, 6 mL) and stirred at 25 °C for 4 h. Removal of the volatiles and a further silica gel column chromatographic purification (ethyl acetate/methanol, 95:5) gave an oil corresponding to **7**α (139 mg) in 72% yield. $[\alpha]^{25}_D$ = +9.6 ($c$ = 1.08, $CHCl_3$/MeOH, 1:1). $^1$H NMR (400 MHz, $CDCl_3$): $\delta$ 1.20 (d, $J$ = 6.4 Hz, 3H), 2.03 (s, 3H), 2.04 (s, 3H), 2.76 (d, $J$ = 4.6 Hz, 3H), 3.53−3.58 (m, 2H), 3.67 (dd, $J$ = 10.9 Hz, $J$ = 1.9 Hz, 1H), 3.90−4.00 (m, 2H), 4.13 (dd, $J$ = 6.0 Hz, $J$ = 2.4 Hz, 1H), 4.38−4.44 (m, 2H), 4.45−4.59 (m, 3H), 4.60−4.65 (m, 1H), 4.73 (d, $J$ = 12.0 Hz, 1H), 4.92−5.00 (m, 2H), 6.18 (d, $J$ = 9.2 Hz, 1H), 6.30−6.35 (m, 1H), 6.42 (d, $J$ = 8.3 Hz, 1H), 7.24−7.38 (m, 15H). $^{13}$C NMR (100 MHz, $CDCl_3$): $\delta$ 17.9, 23.2, 23.4, 26.3, 49.6, 56.7, 69.3, 70.5, 71.5, 72.7, 73.7, 74.4, 76.4, 77.2, 99.7, 127.6, 127.6, 127.7, 127.8, 127.9, 128.2, 128.3, 128.4, 128.5, 137.7, 138.2, 138.4, 170.6, 170.7. Anal. Calcd for $C_{36}H_{45}N_3O_8$: C, 66.75; H, 7.00; N, 6.49. Found: C, 66.64; H, 7.06; N, 6.44.

**Synthesis of Compound 2α.** To a solution of glycoside **7**α (87 mg, 0.13 mmol) in ethyl acetate/methanol (1:1) (10 mL) was added 10% palladium−carbon (40 mg), as a catalyst. The reaction mixture was shaken under $H_2$ (1 atm) for 12 h at 25 °C. Removal of the catalyst and further purification of the residue with C18 reverse-phase sep-pak cartridge gave **2**α (45 mg), as a colorless oil, in 88% yield. $[\alpha]^{25}_D$ = +29.5 ($c$ = 1.46, MeOH). $^1$H NMR (400 MHz, $D_2O$): $\delta$ 1.22 (d, $J$ = 4.0 Hz, 3H) 2.02 (s, 3H), 2.12 (s, 3H), 2.70 (s, 3H), 3.68−3.74 (m, 2H), 3.83 (dd, $J$ = 11.0 Hz, $J$ = 3.1 Hz, 1H), 3.92−4.01 (m, 2H), 4.07 (dd, $J$ = 11.1 Hz, $J$ = 3.8 Hz, 1H), 4.29−4.43 (m, 2H), 4.86 (d, $J$ = 3.8 Hz, 1H). $^1$H NMR (400 MHz, $H_2O/D_2O$, 9:1) for the region of amides: $\delta$ 8.09−8.11 (m, 1H), 8.32 (d, $J$ = 9.5 Hz, 1H), 8.59 (d, $J$ = 8.8 Hz, 1H). $^{13}$C NMR (100 MHz, $CD_3OD$): $\delta$ 18.9, 22.8, 23.1, 27.0, 50.8, 58.9, 62.3, 68.6, 69.5, 72.3, 75.4, 99.5, 173.0, 175.1, 175.9. Anal. Calcd for $C_{15}H_{27}N_3O_8$: C, 47.74; H, 7.21; N, 11.13. Found: C, 47.70; H, 7.20; N, 11.11.

**Synthesis of Compound 6β.** A mixture of **3** (182 mg, 0.78 mmol), NIS (186 mg, 0.83 mmol), 4 Å molecular sieve, and the thiodonor shown in Scheme 1 (302 mg, 0.53 mmol) in $CH_2Cl_2$ (12 mL) was stirred for 1 h sheltered from light at 25 °C under dry Ar, then cooled to 0 °C. TMSOTf (23 $\mu$L, 0.14 mmol) was added, and the mixture was stirred for 20 min at 0 °C and then 12 h at 25 °C. $Et_3N$ (50 $\mu$L) was added, and the mixture was diluted with $CH_2Cl_2$, filtered through a pad of Celite, washed with 5% aqueous $Na_2S_2O_3$, dried ($MgSO_4$), and concentrated. The solvent was removed by evaporation, and the products were separated by flash chromatography on silica gel (ethyl acetate/hexane, 2:3) to give **6**β (75 mg), as a yellow solid, in 20% yield. Mp 162−164 °C; $[\alpha]^{25}_D$ = +33.8 ($c$ = 1.00, MeOH). $^1$H NMR (400 MHz, $CDCl_3$): $\delta$ 1.04 (d, $J$ = 6.4 Hz, 3H), 1.43 (s, 9H), 2.67 (d, $J$ = 4.8 Hz, 3H), 3.58 (d, $J$ = 6.2 Hz, 2H), 3.68−3.74 (m, 1H), 3.94−3.98 (m, 1H), 4.02−4.08 (m, 1H), 4.20−4.30 (m, 2H), 4.44−4.50 (m, 3H), 4.53 (d, $J$ = 11.2 Hz, 1H), 4.61 (d, $J$ = 11.6 Hz, 1H), 4.79−4.94 (m, 3H), 5.53 (d, $J$ = 6.8 Hz, 1H), 6.34−6.39 (m, 1H), 7.25−7.36 (m, 15H). $^{13}$C NMR (100 MHz, $CDCl_3$): $\delta$ 15.7, 26.2, 28.3, 56.9, 67.9, 71.7, 72.5, 73.6, 73.8, 75.0, 77.2, 79.2, 87.6, 100.0, 127.9, 128.0, 128.1, 128.2, 128.3, 128.4, 128.5, 128.5, 128.6, 136.4, 137.4, 137.7, 169.2. Anal. Calcd for $C_{37}H_{47}N_3O_{10}$: C, 64.05; H, 6.83; N, 6.06. Found: C, 64.11; H, 6.80; N 6.02.

**Synthesis of Compound 7β.** Derivative **6**β (150 mg, 0.22 mmol) was dissolved in $CH_2Cl_2$/TFA (1:1, 6 mL), and the solution was stirred at 25 °C for 12 h. The solvent was evaporated, and the residue was dissolved in pyridine/acetic anhydride (2:1, 6 mL) and stirred at 25 °C for 4 h. Removal of the volatiles and a further silica gel column chromatographic purification ($CH_2Cl_2$/methanol, 15:1) gave a white solid corresponding to **7**β (110 mg) in 80% yield. Mp 159−161 °C; $[\alpha]^{25}_D$ = +38.0 ($c$ = 1.05, MeOH). $^1$H NMR (400 MHz, $CDCl_3$): $\delta$ 1.01 (d, $J$ = 6.4 Hz, 3H), 1.98 (s, 3H), 2.72 (d, $J$ = 4.8 Hz, 3H), 3.58−3.63 (m, 2H), 3.77 (t, $J$ = 6.6 Hz, 1H), 3.97−4.01 (m, 1H), 4.08 (dd, $J$ = 10.6 Hz, $J$ = 2.7 Hz, 1H), 4.14−4.23 (m, 1H), 4.43−4.55 (m, 4H), 4.57 (dd, $J$ = 6.2 Hz, $J$ = 3.7 Hz, 1H), 4.61 (d, $J$ = 11.6 Hz, 1H), 4.81−4.89 (m, 2H), 4.98 (d, $J$ = 8.1 Hz, 1H), 6.38−6.43 (m, 1H), 6.59 (d, $J$ = 6.4 Hz, 1H), 7.22−7.39 (m, 15H). $^{13}$C NMR (100 MHz, $CDCl_3$): $\delta$ 15.2, 23.1, 26.2, 55.6, 67.6, 71.6, 72.4, 73.5, 73.8, 75.0, 76.3, 79.1, 87.4, 100.0, 127.7, 127.8, 128.0, 128.2, 128.3, 128.4, 128.4, 128.5, 128.6, 136.4, 137.3, 137.7, 168.7, 170.0. Anal. Calcd for $C_{34}H_{41}N_3O_9$: C, 64.24; H, 6.50; N, 6.61. Found: C, 64.29; H, 6.55; N, 6.57.

**Synthesis of Compound 8β.** Platinized Raney-nickel (T4) catalyst was freshly prepared as described in the literature.[19] The catalyst obtained using 1 g of Raney nickel/aluminum alloy was suspended in ethanol (5 mL) and pre-hydrogenated for 10 min before the addition of **7**β (100 mg, 0.16 mmol) in ethanol (5 mL). The reaction mixture was shaken under $H_2$ (1 atm) for 3 h at 25 °C. The catalyst was filtered off and the solvent evaporated. The residue was dissolved in pyridine/acetic anhydride (2:1, 6 mL) and stirred at 25 °C for 4 h. Removal of the volatiles and a further silica gel column chromatographic purification ($CH_2Cl_2$/methanol, 9:1) gave an oil corresponding to **8**β (46 mg) in 45% yield. $[\alpha]^{25}_D$ = +24.2 ($c$ = 0.58, $CHCl_3$). $^1$H NMR (400 MHz, $CDCl_3$): $\delta$ 1.02 (d, $J$ = 6.4 Hz, 3H), 1.89 (s, 3H), 1.97 (s, 3H), 2.71 (d, $J$ = 4.8 Hz, 3H), 3.59−3.64 (m, 2H), 3.66−3.71 (m, 1H), 3.79−3.99 (m, 3H), 4.13−4.20 (m, 1H), 4.40−4.48 (m, 3H), 4.51−4.55 (m, 1H), 4.58 (d, $J$ = 11.4 Hz, 1H), 4.69 (d, $J$ = 11.9 Hz, 1H), 4.76 (d, $J$ = 8.1 Hz, 1H), 4.91 (d, $J$ = 11.3 Hz, 1H), 5.25 (d, $J$ = 7.7 Hz, 1H), 6.72 (d, $J$ = 6.1 Hz, 1H), 6.74−6.80 (m, 1H), 7.27−7.38 (m, 15H). $^{13}$C NMR (100 MHz, $CDCl_3$): $\delta$ 16.0, 23.3, 23.7, 26.4, 53.7, 56.2, 68.6, 71.9, 72.3, 73.5, 73.7, 74.9, 75.1, 78.2, 101.1, 127.8, 128.0, 128.3, 128.4, 128.6, 128.8, 137.8, 138.0, 138.6, 169.4, 170.2, 170.6. Anal. Calcd for $C_{36}H_{45}N_3O_8$: C, 66.75; H, 7.00; N, 6.49. Found: C, 66.83; H, 7.04; N, 6.47.

**Synthesis of Compound 2β.** To a solution of glycoside **8**β (27 mg, 0.04 mmol) in ethyl acetate/methanol (4:1) (5 mL) was added 10% palladium−carbon (20 mg), as a catalyst. The reaction mixture was shaken under $H_2$ (1 atm) for 7 h at 25 °C. Removal of the catalyst and further purification of the residue with C18 reverse-phase sep-pak cartridge gave **2**β (8 mg), as a colorless oil, in 53% yield. $[\alpha]^{25}_D$ = −0.2 ($c$ = 0.55, $H_2O$). $^1$H NMR (400 MHz, $D_2O$): $\delta$ 1.03 (d, $J$ = 6.2 Hz, 3H), 1.94 (s, 3H), 1.98 (s, 3H), 2.64 (s, 3H), 3.48−3.53 (m, 1H), 3.59 (dd, $J$ = 10.9 Hz, $J$ = 3.3 Hz, 1H), 3.62−3.68 (m, 2H), 3.72 (dd, $J$ = 10.8 Hz, $J$ = 8.5 Hz, 1H), 3.81 (d, $J$ = 3.1 Hz, 1H), 4.16−4.23 (m, 2H), 4.31 (d, $J$ = 8.4 Hz, 1H). $^1$H NMR (400 MHz, $H_2O/D_2O$, 9:1) for the region of amides: $\delta$ 7.79−7.82 (m, 1H), 8.02 (d, $J$ = 7.4 Hz, 1H), 8.14 (d, $J$ = 9.5 Hz, 1H). $^{13}$C NMR (100 MHz, $D_2O$): $\delta$ 18.8, 24.3, 24.7, 28.4, 55.0, 60.6, 63.5, 70.1, 73.3, 77.3, 77.5, 103.0, 174.6, 177.3, 177.5. Anal. Calcd for $C_{15}H_{27}N_3O_8$: C, 47.74; H, 7.21; N, 11.13. Found: C, 47.68; H, 7.18; N, 11.18.

**NMR Experiments.** All the NMR experiments were recorded on a Bruker Avance 400 spectrometer at 293 K, except for the 1D and 2D NOESY spectra of compound **2**α, which were recorded at 278 K on a Varian Unity 500 spectrometer. $^1$H and $^{13}$C NMR spectra were recorded in $CDCl_3$ and $CD_3OD$ with TMS as the internal standard and in $D_2O$ (chemical shifts are reported in ppm on the $\delta$ scale). Magnitude-mode ge-2D COSY spectra were recorded with gradients and using the

cosygpqf pulse program with 90° pulse width. Phase-sensitive ge-2D HSQC spectra were recorded using z-filter and selection before t1 removing the decoupling during acquisition by use of invigpndph pulse program with CNST2 (*J*HC) = 145. 2D NOESY experiments were made using phase-sensitive ge-2D NOESY for $CDCl_3$ spectra and phase-sensitive ge-2D NOESY with WATERGATE for $H_2O/D_2O$ (9:1) spectra. Selective ge-1D NOESY experiments were carried out using the 1D-DPFGE NOE pulse sequence. NOE intensities were normalized with respect to the diagonal peak at zero mixing time. Experimental NOEs were fitted to a double exponential function, $f(t) = p_0(e^{-p1t})(1 - e^{-p2t})$ with $p_0$, $p_1$, and $p_2$ being adjustable parameters.[12] The initial slope was determined from the first derivative at time $t = 0$, $f'(0) = p_0p_2$. From the initial slopes, interproton distances were obtained by employing the isolated spin pair approximation.

**Molecular Dynamics Simulations.** MD-tar simulations were performed with AMBER[20] 6.0 (parm94),[21] which was implemented with GLYCAM 04 parameters[22] to accurately simulate the conformational behavior of the sugar moiety. NOE-derived distances were included as time-averaged distance constraints, and scalar coupling constants *J* as time-averaged coupling constraints. A $<r^{-6}>^{-1/6}$ average was used for the distances, and a linear average was used for the coupling constants. Final trajectories were run using an exponential decay constant of 8000 ps and a simulation length of 80 ns for the MD-tar simulation with $\epsilon = 80$, and using an exponential decay constant of 400 ps and a simulation length of 4 ns for the MD-tar simulations in explicit water.

**DFT and NBO Calculations.** All calculations were carried out using the B3LYP hybrid functional.[23] The 6-31G(d) basis set was used in the full optimization of **2**α together with its first hydration shell, and the 6-31G(d,p) basis set was used for the scans. In the case of reduced models of **1**α and **2**α (see Supporting Information), full geometry optimizations and relaxed potential energy surface (PES) scans with step sizes of 5° were carried out using the Gaussian 03 package.[24] BSSE corrections were not considered in this work. Frequency analyses were carried out at the same level used in the geometry optimizations, and the nature of the stationary points was determined in each case according to the appropriate number of negative eigenvalues of the Hessian matrix. Scaled frequencies were not considered since significant errors in the calculated thermodynamical properties are not found at this theoretical level.[25] Electronic energies ($\Delta E$'s) were used for the discussion on the relative stabilities of the considered structures. Steric interactions were evaluated by means of the pairwise steric exchange energies for disjoint interactions.[26] Delocalizing interactions (hyperconjugation) were stimated by calculating the second-order perturbation energies.[27] These quantities were calculated through a natural bond orbital/natural localized molecular orbital (NBO/NLMO) analysis using the NBO 5.G program[18] and upgraded Gaussian 03 as interface. These attractive and repulsive interactions were estimated by means of the localized $\sigma$, $\pi$, n, $\sigma^*$, and $\pi^*$ valence orbitals.

**Acknowledgment.** We thank the Ministerio de Educación y Ciencia and FEDER (Project CTQ2006-05825 and Ramón y Cajal contracts of F.C. and J.H.B.), the Universidad de La Rioja (Project API-05/B01 and grants of G.J.-O. and M.G.L.), and the Gobierno de La Rioja (ANGI-2004/03 and ANGI-2005/01 projects). We also thank CESGA for computer support.

**Supporting Information Available:** $^1H$ and $^{13}C$ NMR spectra, as well as COSY, HSQC, and 2D-NOESY correlations, of compounds **1**$\beta$, **2**α, and **2**$\beta$; 1D NOE selective spectra for compound **2**α; TOCSY and 2D *J*-resolved correlations for compound **2**$\beta$; MD simulations in explicit water for derivative **2**α; torsional barrier for $\psi_s$ in **1**α and **2**α derived from AMBER/GLYCAM force field; NBO analysis of reduced model of **1**α and **2**α; B3LYP/6-31G(d) distances, dihedral angles, energy, enthalpy, free energy, entropy, and coordinates of the optimized structure of **2**α together with its first hydration shell; complete refs 20b and 24. This material is available free of charge via the Internet at http://pubs.acs.org.

JA072181B

(20) (a) Pearlman, D. A.; Case, D. A.; Caldwell, J. W.; Ross, W. R.; Cheatham, T. E., III; DeBolt, S.; Ferguson, D.; Seibel, G.; Kollman, P. *Comput. Phys. Commun.* **1995**, *91*, 1−41. (b) Kollman, P. A., et al. *AMBER 6*; University of California: San Francisco, 1999.
(21) Cornell, W. D.; Cieplack, P. C.; Bayly, I.; Gould, I. R.; Merz, K.; Ferguson, D. M.; Spellmeyer, D. C.; Fox, T.; Caldwell, J. W.; Kollman, P. A. *J. Am. Chem. Soc.* **1995**, *117*, 5179−5197.
(22) Woods, R. J.; Dwek, R. A.; Edge, C. J.; Fraser-Reid, B. *J. Phys. Chem. B* **1995**, *99*, 3832−3846.
(23) (a) Lee, C.; Yang, W.; Parr, R. *Phys. Rev. B* **1988**, *37*, 785−789. (b) Becke, A. D. *J. Chem. Phys.* **1993**, *98*, 5648−5652.
(24) Pople, J. A., et al. *Gaussian 03*, revision B.05; Gaussian, Inc.: Pittsburgh, PA, 2003.
(25) Bauschlicher, C. W., Jr. *Chem. Phys. Lett.* **1995**, *246*, 40−44.
(26) (a) Badenhoop, J. K.; Weinhold, F. *J. Chem. Phys.* **1997**, *107*, 5406−5421. (b) Badenhoop, J. K.; Weinhold, F. *J. Chem. Phys.* **1997**, *107*, 5422−5432. (c) Badenhoop, J. K.; Weinhold, F. *Int. J. Quantum Chem.* **1999**, *72*, 269−280.
(27) (a) Reed, A. E.; Curtiss, L. A.; Weinhold, F. *Chem. Rev.* **1988**, *88*, 899−926. (b)Weinhold, F. In *Encyclopedia of Computational Chemistry, Vol. 3: Natural Bond Orbital Methods*; Schleyer, P. v. R., Ed.; 1998; pp 1792−1811.